Landslide Dam Failure Analysis Using Imaging and Ranging Sensors

Keivan Tavakoli[1], Ehsan Zadehali[1], Arsalan Malekian[1], Sara Darsi[1], Laura Longoni[2], and Marco Scaioni[3](✉)

[1] Politecnico di Milano, Lecco Campus, via G. Previati 1/c, 23900 Lecco, Italy
{keivan.tavakoli,ehsan.zadehali,arsalan.malekian,
sara.darsi}@mail.polimi.it
[2] Department of Civil and Environmental Engineering, Politecnico di Milano,
piazza L. da Vinci 32, 20133 Milano, Italy
laura.longoni@polimi.it
[3] Department of Architecture, Built Environment and Construction Engineering,
Politecnico di Milano, via Ponzio 31, 20133 Milano, Italy
marco.scaioni@polimi.it

Abstract. Landslide dam failure may be triggered by heavy rainfall or earthquake and may fail due to seepage or piping because of the asymmetric compaction. Hence, they have the potential to result in serious natural hazards. Rapid assessment of this phenomenon requires the application of investigation and monitoring techniques providing information on the ongoing failure process. To this aim, a downscaled model of a natural dam landslide was reconstructed in a simulation facility (the 'Landslide Simulator') located in the Lecco Campus of Politecnico di Milano university, Italy. The failure of the dam was induced by artificial rainfall. A sensor network was setup to record observations during the simulation experiment, including geotechnical, geophysical, and imaging/ranging sensors. This paper focuses on the analysis of deformation measurement and other changes over time, which were observed in the recorded image sequences and 3D point clouds to analyze and predict the failure of the dam. Results showed that water seepage may play a dominant role in the dam failure process, which is anticipated by a sharp increase of strain in the dam body. Furthermore, image processing techniques may help scientists to calibrate numerical models to improve their quality and reliability.

Keywords: Digital image correlation · Landslide dam failure · Monitoring · Sensor network · Terrestrial laser scanning

1 Introduction

Climate factors and/or geological processes may generate natural dams, including landslide dams, glacier dams, moraine dams as classified by Costa and Schuster [4].

Among these, landslide dams may be generated by earthquakes or heavy rainfall events [21]. Because the accumulated material that creates a landslide dam comes mainly

© Springer Nature Switzerland AG 2021
O. Gervasi et al. (Eds.): ICCSA 2021, LNCS 12955, pp. 3–17, 2021.
https://doi.org/10.1007/978-3-030-87007-2_1

from the surrounding mountain and is not artificially stabilized, it is much looser, less compact, and has lower cohesive strength than earth artificial dams. This condition makes landslide dams more susceptible to burst failure, potentially leading to catastrophic flooding in the downstream region.

A landslide dam in its natural state is made up of a heterogeneous mass of poorly consolidated earth material and has no channelized spillway or other protected outlets. Due to these reasons, landslide dams commonly fail by overtopping, followed by breaching from erosion by the overflowing stream, as reported in an exhaustive study by Costa and Schuster [4], who analyzed the failure of 73 landslide dams known up to-date (see Fig. 1). In most cases, the breach is the result of the fluvial erosion of the landslide material by head cutting generating at the toe of the dam and progressively moving upstream towards the basin. When the head cut reaches the lake, breaching occurs [18]. Smaller lakes may remain after dam failure because the breach commonly does not erode down to the original river level. In some situations, the landslide dam will not fail during first filling and overtopping. Subsequent failure may occur by surface erosion accompanying unusually large runoff periods. This was the case in the failure of the landslide dams at Lower Gros Ventre, Wyoming, and Val Pola [1–29].

Because landslide dams have not undergone systematic compaction, they may be porous, and seepage through the dams potentially could also lead to collapse by internal erosion (piping). On the downstream slope of many landslide dams, seeps have been noted. Examples is the Cerro Condor-Seneca landslide dam in Peru, which failed in 1945, probably because of "violent" seepage and piping [30].

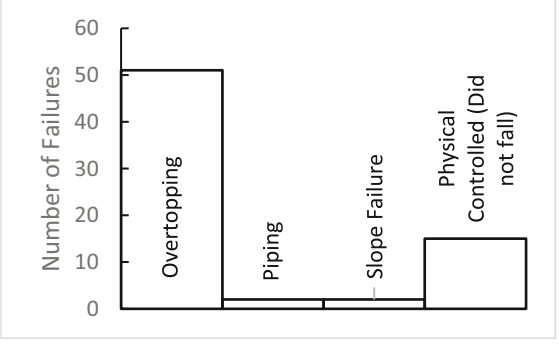


Fig. 1. Graph showing modes of failure of natural landslide dams, based on 55 failures from the literature and the authors' experience [4].

The most critical consequence of the landslide dam failure is flooding, which may result in devastating effects on the population, the urban, industrial and rural settlements, the infrastructures and the social/economic activity in the downstream area of the dam due to the discharge of water and sediments. Flooding may develop in both upstream (backwater) direction as the impoundment fills, and downstream direction because of the failure of the dam. Schuster [28] also reports some mitigation measures to reduce the risk related to flooding. These measures aim at controlling the water flow using different strategies [22].

On the other hand, especially the downstream flooding depends upon the stability of the landslide dam. An accurate monitoring of its geotechnical conditions may help understand and predict a potential collapse. Several techniques have been developed and tested for monitoring the safety condition of man-made dams, including the use of geotechnical and in-situ deformation sensors for investigating the inner part of the structure, as well as geodetic and remote sensing methods for detection of surface displacements [27]. In the case of landslide dams that have a casual nature and an unorganized structure, the establishment of permanent sensor networks may be more involved. On one side, because it would require some time before a monitoring network might become operational. On the other hand, because landslide dams may present a complex topographic surface and are not generally provided with infrastructures to access them with easy.

The use of remote sensing techniques from satellite (i.e., Differential Interferometric Synthetic Aperture Radar – DInSAR – [20], unmanned aerial vehicles (drone photogrammetry [11], and the ground surface (terrestrial laser scanning, Ground-based InSAR [13–15] platforms represent a valid solution to collect data for monitoring the safety conditions of the landslide-dam body and the basin, especially in the immediate post-disaster time. To this purpose, imaging and ranging sensors may be rapidly applied to predict possible failures and warn everyone to suffer less damage [34].

The limited availability of documented events makes quite difficult to understand the dynamics of landslide-dam failure processes in order to model them for prediction [7]. An alternative approach for investigating this problem may be found in laboratory simulations on downscaled models, which have been already exploited in landslide research [9–26]. Xu [33] showed that the development of the discharge channel and the failure of a landslide dam may be simulated in laboratory and monitored by digital cameras. Experimental results revealed that the upstream inflow and the dam size are the main factors that impact the dam break process. The peak flow may be reduced by an excavated discharge channel with trapezoidal section. The depth of the discharge channel may significantly influence the dam-break process.

In recent years, some experimental research activities have been undertaken at Lecco Campus of Politecnico di Milano (Italy) to investigate the relationship of earth slope stability and water infiltration due to rainfall [31]. This process has been physically simulated at smaller scale in a 'Landslide Simulator,' see Sect. 2.1. This facility is used in both research projects and teaching activities of the MSc course on Civil Engineering for Risk Management [25].

In this research, a landslide dam has been reproduced and infiltrated by water located in a basin in the upstream surface. Some geotechnical, geophysical and imaging/ranging sensors have been used to collect data useful to predict the failure sequence of the landslide dam. This paper is focused in particular on the analysis of imaging and ranging data.

2 Experimental Setup

2.1 The 'Landslide Simulator'

A 'Landslide Simulator' consists of a flume where a downscaled earth slope may be reconstructed and a landslide physically simulated. Within a such facility, rainfall may

be induced as triggering factor, while the slope inclination may be controlled to analyze how it may influence the slope stability. The main goal of the 'Landslide Simulator' built up at Lecco Campus of Politecnico di Milano is to investigate the modes of collapse of earth slopes and the factors which may control this kind of processes: rainfall intensity, material property, discharge flow, initial moisture content, as well as gradient of the inclined topographic surface and geometrical properties of the slope [23]. The 'Landslide Simulator' is composed of two adjustable metallic surfaces, as shown in Fig. 2a. The upper part of the flume has dimensions 2 m $\times$ 0.8 m and could be lifted up to an inclination of 45°. During the experiment presented in this paper, it was lifted up to an inclination of 20°. Geogrid is supplied at the bottom to maintain friction between soil and structure, whilst the lateral sides of the flume are made of transparent plexiglass to allow the visual evaluation of the inner slope. A water distribution system is located in the upper side of the flume, from where artificial rainfall can be poured down.

The 'Landslide Simulator' has been equipped with different types of sensors, including geotechnical, geophysical and some digital cameras in different positions, while a total station (TS) and a terrestrial laser scanner (TLS) are used in front of it (see Fig. 2b). The TS is adopted for georeferencing different data sets into a common topographic reference system, while TLS is applied to collect point clouds to record the surface of the downscaled model at different times during the simulation experiment.

2.2 The Downscaled Model of a Natural Landslide Dam

In the experiment described in this paper a natural landslide dam has been simulated. The adopted material is made of medium-size sand with 26.2 kN/m^3 specific weight, zero cohesion and internal friction of 35°. The dam has dimensions of 30 cm high at the crest and 110 cm in length. The downstream slope is 1/2 and the upstream slope is 3/4, which gives a steep slope at the side where failure may occur (see Fig. 2a).

2.3 The Sensor Network

Progressively, by adding water in the basin behind the dam, water infiltration has developed and led to the collapse of the embankment. During this process, a sensor network has been used to record data for monitoring purpose. Adopted sensors can be split in three groups: (1) geotechnical sensors; (2) geophysical sensors; and (3) imaging and ranging sensors. Environmental parameters have not been recorded, since they did not significantly influence the experiment. Each sensor technology is provided with its own data logger device. Some outputs may be displayed in real time during the experiment, but the main purpose is to record all observations and to process them offline.

Geotechnical sensors (1) consist of two tensiometers for measuring pore-water pressure, which have been installed in the upstream and downstream slopes (Fig. 2c).

Geophysical sensors (2) are employed for resistivity measurements. A system based on two 24-channel mini-cables assembled in-house and terminated with 48 stainless-steel 2 cm-long mini-electrodes has been tentatively installed [2]. A practical problem of cable failure resulted in the positioning of 41 cables only. These are consistent with the commercial IRIS Syscal Pro instrument (www.iris-instruments.com). The electrode configuration used in both profiles has been a Wenner array. In this way, 24 electrodes

with interdistance 3 cm have been installed in Profile A (downslope), while 17 electrodes with 4.5 cm spacing in Profile B.

Group (3) of sensors consisted of two different technologies. A TLS FARO Focus 3D X330 has been used during the landslide simulation experiment to collect 3D point clouds of the dam surface. Due to its very-high scanning speed, the acquisition of a point cloud covering the full downscaled model could be accomplished in approx. 1 min. The point density of the point cloud was quite high, with an average point spacing of 2 mm. The FARO Focus 3D X330 is equipped with an internal levelling sensor able to define the z-axis of the intrinsic reference system of the adopted point cloud along the local plumb line [32]. A TS has been also adopted for georeferencing data into the topographic reference frame (Fig. 2b). Figure 3 shows that due to the presence of tensiometers and mini-cables for geoelectrical resistivity measurements, TLS data were affected by some occlusions.

A couple of digital cameras YiCameras by XiaoYi (16 Mpixels sensor, 155° view angle) have been installed for image acquisition from the top of the landslide dam. The installation of low-cost grade cameras has been motivated by the critical condition inside the flume, which may lead to damaging the imaging sensors. As visible in Fig. 2d, a grid has been painted on one side of the downscaled dam model to measure the inner deformation field by using images collected by a single-lens-reflex (SLR) camera Nikon D700 equipped with a 28 mm lens. An additional mirror-less camera Nikon V1 has been placed in front of the 'Landslide Simulator' to record time-lapse images for documenting the whole experiment. Since multiple monitoring sensors have been deployed in the downscaled dam, such as resistivity measurement electrodes and tensiometers, attention has been paid not to limit the field-of-view of the imaging sensors. Despite of this, some mini-cables for georesistivity measurement have resulted in some occlusions in the images, as shown in Fig. 3.

All adopted cameras have been used to record image sequences for documentation purpose. One of the action cameras hang in upper position and the lateral SLR camera have been used for digital image correlation (DIC) analysis, as described in next section. In this experiment, no 3D photogrammetric reconstruction has been accomplished due to the concurrent use of TLS to provide accurate 3D point clouds [23].

3 Methods

3.1 Digital Image Correlation

The evaluation of surface displacements from image sequences has been retained suitable for the prediction of slope failures [24], while the volumetric changes have been evaluated using TLS data. In particular, the image sequences obtained from time-lapse acquisition have been processed using 2D digital image correlation (2D DIC) [8]. The concept of DIC is to track surface displacements by selecting a grid of correlation windows, whose size and spacing may be selected case-by-case.

The DIC analysis has been carried out by multiple commercial and open-source software packages with the aim of comparing their results with each other. The first group comprehended VIC-2D® ver. 6 (www.correlatedsolutions.com) and GOM Correlate® (www.gom.com), which are offered in 30-days free trial-demo version that may be used



Fig. 2. (a) The landslide 'Landslide Simulator' and the sensor network with two adjustable metallic surfaces and natural landslide dam model made up of homogeneous sand; (b) different kind of sensors, cameras, and monitoring devices (in particular terrestrial laser scanning – TLS and total station – TS); (c) sensor network deployment: cameras installed over the model (top red circle), tensiometer installed in the downstream slope (down red circle), and mini-cables for resistivity measurement (red arrow); (d) grid painted on the model's side and lateral single-lens-reflex (SLR) camera (Color figure online).

by students to accomplish their experiments during classes. VIC-2D® is an innovative system implementing the DIC technique to provide strain measurements through 2D contour maps for planar surface specimens. GOM Correlate® is a software package that can be used for 2D/3D (in this research we just used GOM-3D) DIC and motion analysis in material and component testing. The open-source MATLAB® code for 2D DIC by Eberl [6] has been also applied.

After choosing the area of interest to be analyzed, the position of correlation windows is compared at different times (Fig. 4a and b). The rate of image acquisition has been setup to record one image every 30 s.

DIC outputs consisted of displacements and strains that can be visualized at different time. AutoCAD (Student Edition-2019) Autodesk® software has been used to display the final deformation fields obtained from DIC.

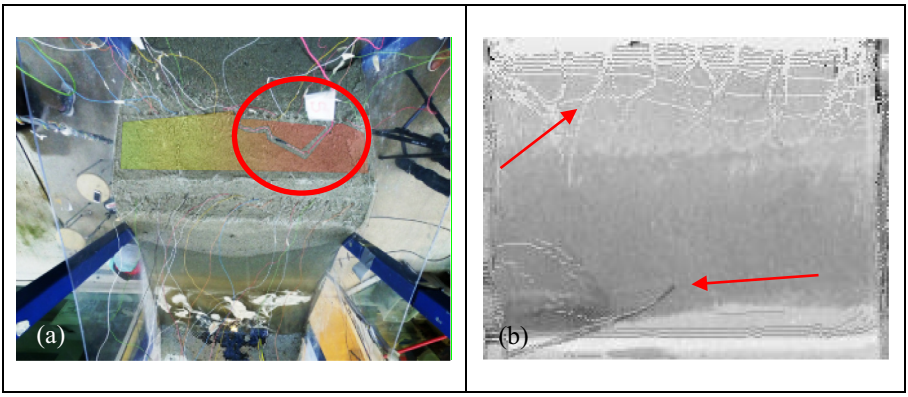


Fig. 3. (a) Data gaps due to the copresence of multiple sensors: (a) effect of the of wires in the results from 2D-DIC (digital image correlation) analysis (red circle); (b) effects of the wires (top arrow) and tensiometer (down arrow) in the point cloud obtained from TLS measurements.

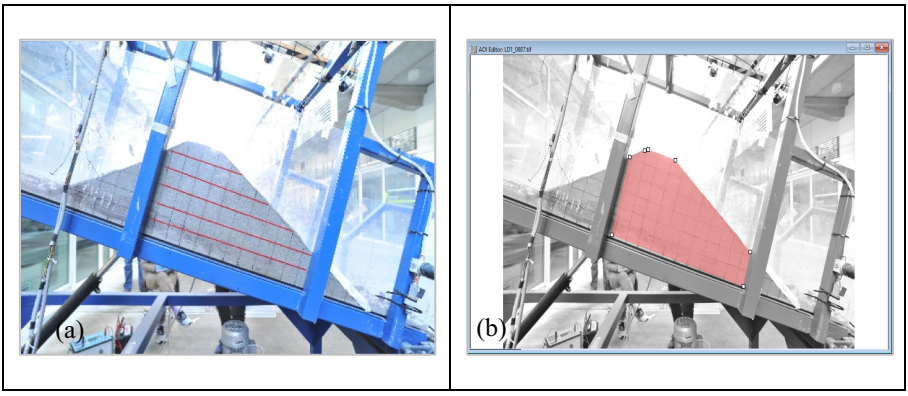


Fig. 4. Selected area of interest for DIC. Red dots show the initial positions of correlation window in the case of MATLAB code (a) and VIC-2D® (b)

3.2 Point Cloud Processing

The open-source CloudCompare software in its latest stable version (ver. 2.11.3 'Anoia') has been used for processing point clouds collected by TLS (www.cloudcompare.org). This popular software allows to directly import scans recorded by FARO Focus 3D X330, to apply pre-processing tasks (data cleaning, subsampling, filtering), to co-register/georeferencing multiple scans, and to compute changes between pairs of aligned scans [19]. About the last operation, CloudCompare offers several methods to compute distances between two point clouds (see Sect. 4.2) or volumes between them (see Sect. 4.3).

4 Results

4.1 Image Processing for Calibration of the Numerical Model

One of the most important application of image processing in laboratory experiments is to record data useful for the calibration of numerical models [8]. In this research, 2D DIC provided experimental information on the dam's deformation and the strain field on the downstream slope and the right hydrographic side of the landslide dam. The lateral image sequence from the SLR Nikon 700 camera was used for visually detecting the variation of the water level in the basin and correlate it with the water infiltration in the body of the landslide dam.

Though the same processing technique (DIC-2D) has been applied with different software packages, outputs have not been the same. For example, VIC-2D® and open-source 2D DIC code by Eberl [6] have been successfully used to process a sequence of 71 images recorded by the side SLR camera. This data set spans from the beginning of the experiment up until the appearance of first crack observed by the side SLR camera.

The application of 2D-DIC in the sequence of 71 images from the lateral camera has provided a map of Von Mises strain during the experiment. Figure 5a shows that the value of strain increased within time because of the gradual infiltration of water in the upstream side (see the area 'A1' in the red circle). Before the appearance of first crack, a new area ('A2') with high value of strain appears (see Fig. 5a), which may be useful to predict the first crack (Fig. 5b).

This visual outcome has been confirmed by the average strain values measured at the same time, which are reported in Fig. 6. This plot shows that before the appearance of first crack, the average strain has sharply skyrocketed.

The application of GOM-3D Correlate® with the same data set has not provided acceptable results, probably due to the image configuration and the distance of dam from cameras and the presence of some wires resulting in occlusions. Indeed, as far as those sequences recorded by the YiCameras placed over the downscaled dam is concerned, the presence of the mini-cable electrodes for georesistivity measurements have prevented the successful application of GOM-3D Correlate® (Fig. 7).

4.2 Point-Cloud Analysis

In this subsection, the evaluation of surface changes of the dam body obtained from the comparison of point clouds collected by TLS are illustrated. The open-source software CloudCompare has been used to this purpose. A set of three point clouds (see Fig. 8) have been considered, whose acquisition was accomplished before the experiment (Point cloud 'a'), after the opening of the first crack on the dam downstream face (Point cloud 'b'), and after the dam failure (Point cloud 'c').

First of all, point clouds have been registered together in the same reference system. This task has been carried out by cascading two methods: (1) matching bounding-box centers for the approximate alignment of two point clouds; and (2) Iterative Closest Point (ICP) registration algorithm to refine the alignment [3].

CloudCompare software implements different methods to compare point clouds in a pairwise manner [5]:

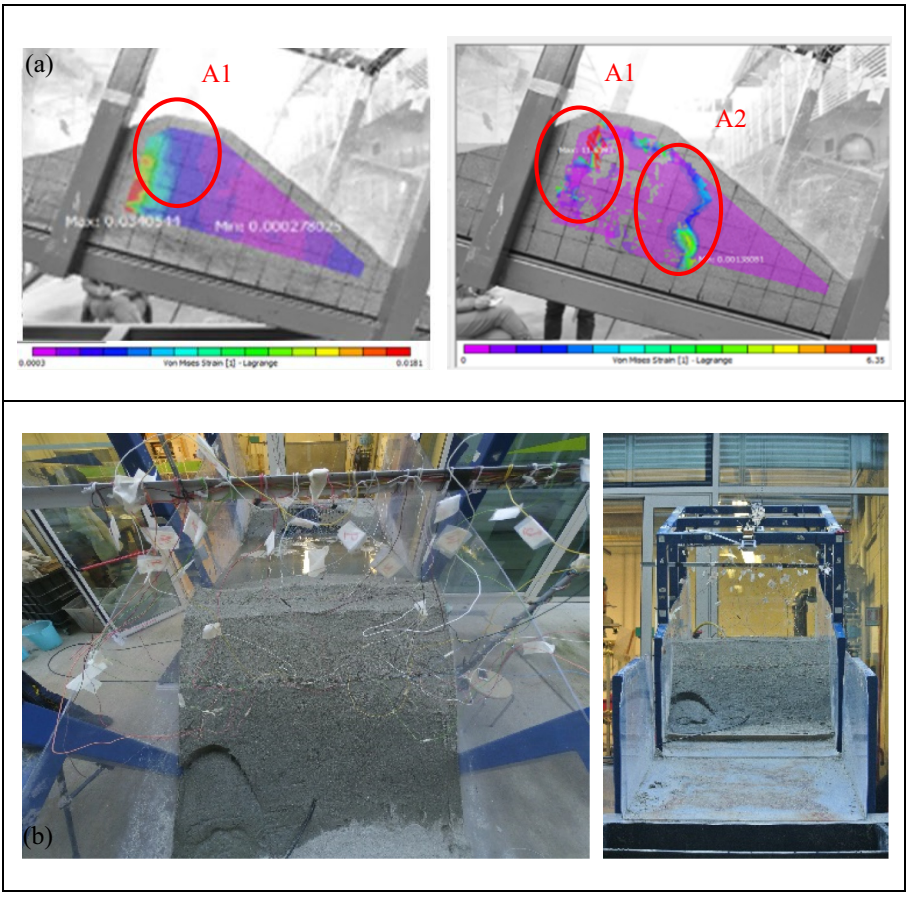


Fig. 5. Comparing the place of first crack and the position of area with high strain (a). The result of VIC-2D at time = 16:15 (left figure) and at time = 16:36, one minute before the first crack (right figure). (b) Top and front image which show the first crack at time 16:37.

- 'Cloud-to-Cloud' (C2C): distances between points from both 'reference' and 'compared' point clouds are considered;
- 'Cloud-to-Mesh' (C2M): distances between points from the 'compared' point cloud and a triangular (TIN – Triangulated Irregular Network) mesh interpolating the 'reference' point cloud are considered;
- 'Mesh-to-Mesh' (M2M): distances between triangular meshes derived from both 'reference' and 'compared' point clouds are considered; and
- 'Multiscale Model-to-Model Cloud Comparison' [17]: this algorithm computes local normals in the 'reference' point cloud and detect those points from the 'compared' point cloud that fall inside a cylinder parallel to the normal. Planes (or other regular surfaces) are estimated from both selected point sets, and the distance between these surfaces considered for measuring the distance between point clouds in that location.

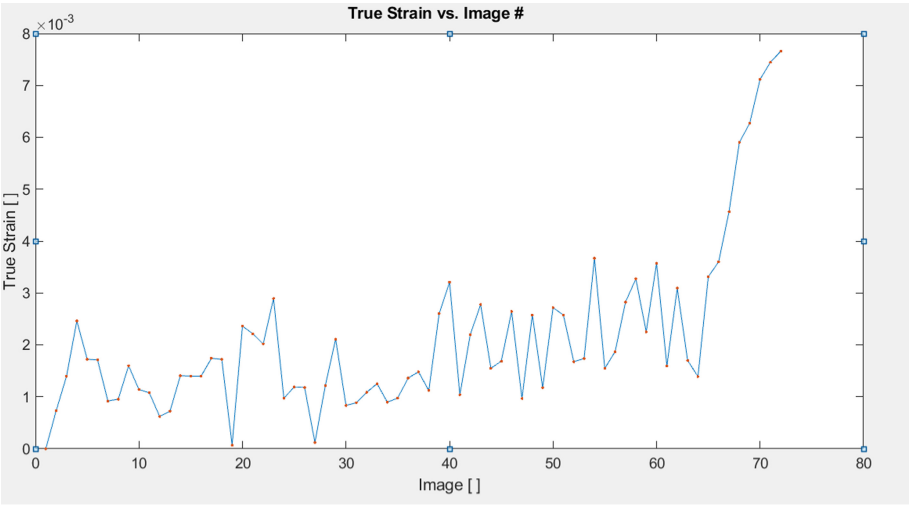


Fig. 6. Average value of measured strains obtained from DIC during the experiment.

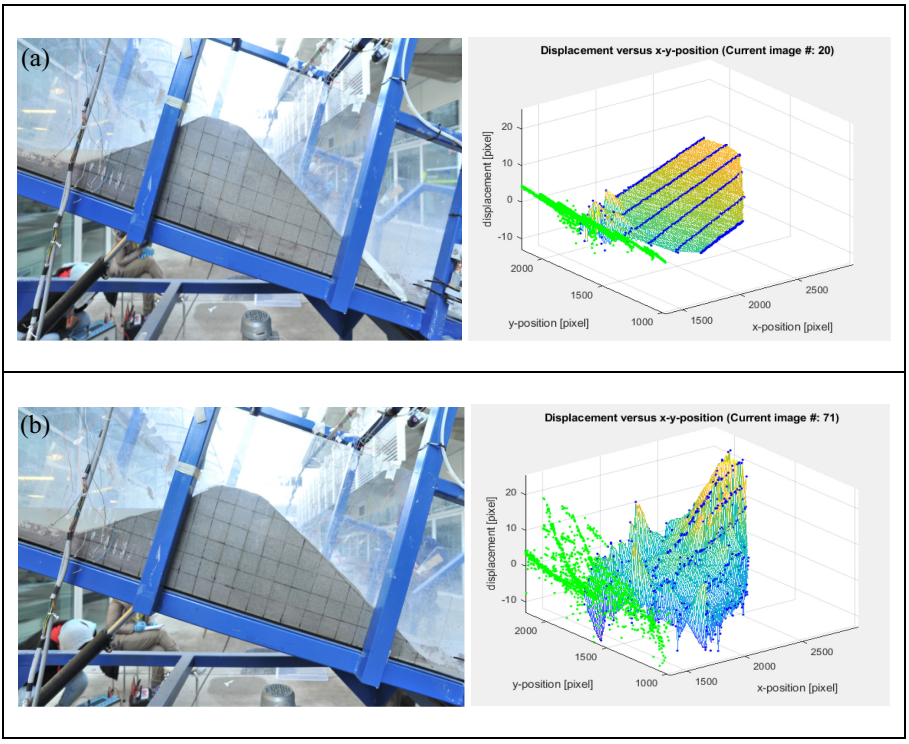


Fig. 7. (a) Displacement from Image 20 (b) Displacement from Image 71.

M3C2 algorithm also estimates the local noise and (optionally) may be input the registration error to detect a significant Level-of-Detection (LoD) for changes [10].

The selection of one method depends on the surface geometry of the object, the point resolution and noise, the direction of expected displacements (e.g., preferably in the normal or tangential directions with respect to the 'reference' point cloud), and the presence of subregions with displacements in different orientations. In addition, the 'C2C' method cannot provide signed distances since points cannot define a positive direction, such as surfaces may do.

Point clouds 'b' and 'c' have been compared to point cloud 'a' used as 'reference'. Considering the expected homogeneous direction of the surface displacements, the 'C2C' method has been applied. Results are visually mapped in Fig. 9.

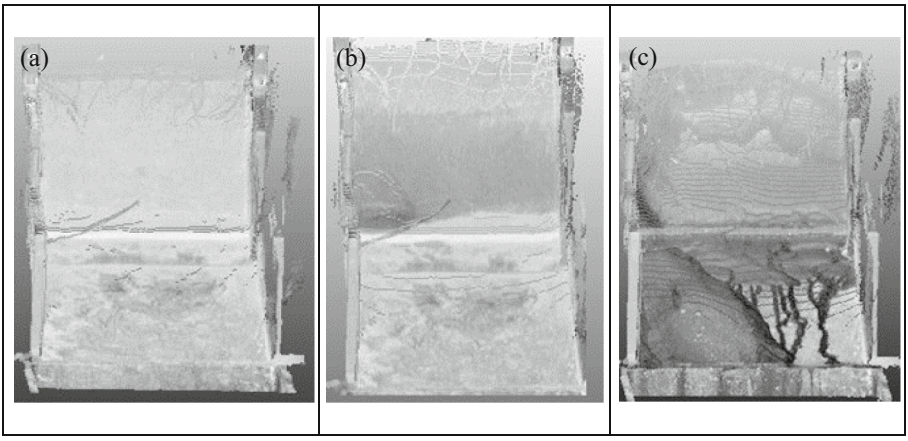


Fig. 8. Visualization of point clouds collected by using TLS at different phases of the experiment: (a) landslide dam without deformation at the beginning of the experiment; (b) appearance of first crack; and (c) after dam failure.

4.3 Computing Volume Change

After registration and comparison between point cloud surfaces, volumetric change has been analyzed to understand how much sediment has been lost during the different stages of the dam failure process. Indeed, the dam breaching resulted in the generation of a rapid mud flow able to transport a huge amount of sediment.

A function implemented in CloudCompare has been applied to compute volume between point clouds, requiring the selection of a reference surface. In this case, the bottom surface of the flume has been chosen to this purpose.

This analysis has highlighted that between situations (a) and (b) reported in Fig. 10, which corresponded to the initial undeformed condition, and the post-breaching, 5.3% of total volume has been removed from the body of the landslide dam in the meanwhile between both epochs. By comparing the sediment volume in the downstream region, it

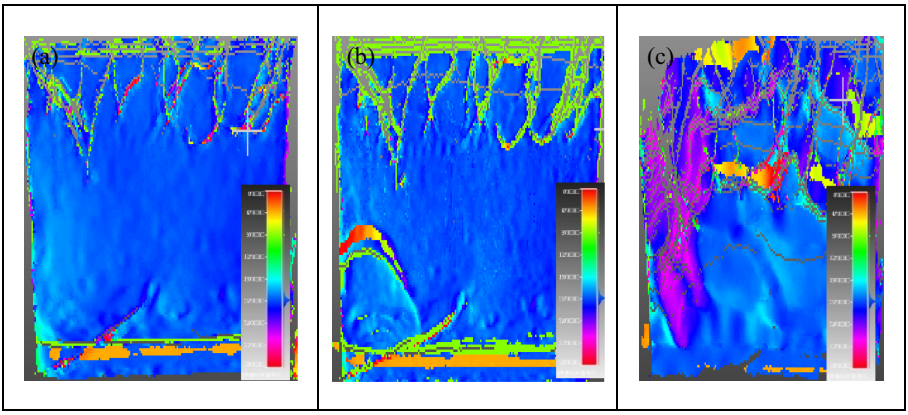


Fig. 9. Local orientation of each cell in the point clouds collected at different epochs: (a) dam without deformation; (b) appearance of first crack; and (c) after dam breaking.

has been detected that approx. 1.1% of the total volume has been deposited, and approx. 0.042% has been moved away by water. This amount of sediment has collapsed as debris flow.

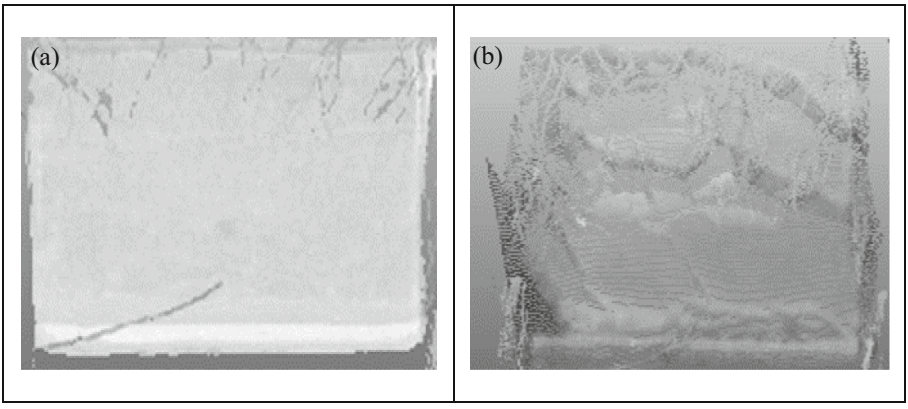


Fig. 10. Point clouds illustrating the conditions of the landslide dam at both epochs considered for computing volume change: (a) before deformation start; (b) after dam breaking.

5 Conclusion

In this paper the problem of landslide dam failure has been studied by reproducing a downscaled model in a laboratory facility ('Landslide Simulator') established on the Lecco Campus of Politecnico di Milano university, Italy. The process has been observed and monitored by adopting a sensor network including geotechnical and geophysical

in-situ sensors, integrated by some imaging and ranging sensors. In particular, in this paper this last category of observations has been focused.

Imaging sensors consisted of a couple of action-grade cameras installed above the downscaled model to investigate surface displacements by means of 2D Digital Image Correlation (DIC). An additional single-lens-reflex camera has been placed to collect an image sequence of the lateral side of the landslide dam body through a transparent panel. In this way, the 2D-DIC on the inner layers of the dam in contact with the lateral glass could be investigated to detect the water seepage process, to be correlated to the level of water in the upstream basin. The results show that by using 2D-DIC, strain and displacements could be measured and the sudden acceleration of these two parameters could be useful for predicting the failure of the landslide dam. Furthermore, a relationship has been found between the quantity of water infiltrated on the upstream body of the dam and surface displacements.

A phase-shift terrestrial laser scanner for medium range data acquisition has been used for collecting 3D point clouds at significant epochs of the experiment run. By a point cloud management and processing software (CloudCompare), surface changes and volumes have been computed. By considering volume changing before and after dam failure, the volume of sediment that has flown away corresponded to approx. 28% of the whole sand volume in the landslide dam body. This sediment flow might be main reason of direct damage in a real-world failure.

Acknowledgements. The authors would like to acknowledge companies that provided free trial-demo version of software packages VIC-2D® and GOM Correlate® to allow students to accomplish their experiments. They would like also to acknowledge Eberl [6] for the open-source Matlab® code for 2D DIC and the authors of CloudCompare open-source software. Eventually, acknowledgements go to the Lecco Campus of Politecnico di Milano and to Prof. Monica Papini for the availability of the 'Landslide Simulator'.

References

1. Alden, W.C.: Landslide and flood at Gros Ventre, Wyoming. In: Tank, R. (ed.) Focus on Environmental Geology (1928)
2. Hojat, A., et al.: Quantifying seasonal 3D effects for a permanent electrical resistivity tomography monitoring system along the embankment of an irrigation canal. Near Surf. Geophys. **18**, 427–443 (2020). https://doi.org/10.1002/nsg.12110
3. Besl, P.J., McKay, N.D.: Method for registration of 3-d shapes. In: Sensor Fusion IV: Control Paradigms and Data Structures, pp. 586–560. International Society for Optics and Photonics. https://doi.org/10.1109/34.121791 (1992)
4. Costa, J.E., Schuster, R.L.: The formation and failure of natural dams. USGS Open-File, Report 87-392, https://doi.org/10.3133/ofr87392 (1987)
5. DiFrancesco, Paul-Mark., Bonneau, D., Hutchinson, D.J.: The implications of M3C2 projection diameter on 3D semi-automated Rockfall extraction from sequential terrestrial laser scanning point clouds. Remote Sens. **12**(11), 1885 (2020). https://doi.org/10.3390/rs12111885
6. Eberl, C.: MATLAB Central File Exchange. Digital Image Correlation and Tracking. https://www.mathworks.com/matlabcentral/fileexchange/12413-digital-image-correlation-and-tracking (2021)

7. Ermini, L., Casagli, N.: Prediction of the behaviour of landslide dams using a geomorphological dimensionless index. Earth Surf. Proc. Land. **28**, 31–47 (2003). https://doi.org/10.1002/esp.424
8. Fedele, R., Scaioni, M., Barazzetti, L., Rosati, G., Biolzi, L., Condoleo, P.: Delamination tests on CFRP-reinforced masonry pillars: optical monitoring and mechanical modelling. Cement Concr. Compos. **45**, 243–254 (2014). https://doi.org/10.1016/j.cemconcomp.2013.10.006
9. Feng, T., et al.: Measurement of surface changes in a scaled-down landslide model using high-speed stereo image sequences. Photogrammetr. Eng. Remote Sens. **82**(7), 547–557 (2016). https://doi.org/10.14358/PERS.82.7.547
10. Fey, C., Wichmann, V.: Long-range terrestrial laser scanning for geomorphological change detection in alpine terrain – handling uncertainties. Earth Surf. Proc. Land. **42**, 789–802 (2017). https://doi.org/10.1002/esp.4022
11. Giordan, D., Manconi, A., Remondino, F., Nex, F.: Use of unmanned aerial vehicles in monitoring application and management of natural hazards. Geomat. Nat. Haz. Risk **8**, 1–4 (2017). https://doi.org/10.1080/19475705.2017.1315619
12. Glazyrin, G.Y., Reyzvikh, V.N.: Computation of the flow hydrograph for the breach of landslide lakes. Soviet Hydrol. **5**, 492–496 (1968)
13. Gonzalez-Aguilera, D., Gomez-Lahoz, J., Sanchez, J.: A new approach for structural monitoring of large dams with a three-dimensional laser scanner. Sensors **8**, 5866–5883 (2008). https://doi.org/10.3390/s8095866
14. Hänsel, P., Schindewolf, M., Eltner, A., Kaiser, A., Schmidt, J.: Feasibility of high-resolution soil erosion measurements by means of rainfall simulations and SfM photogrammetry. Hydrology **3**(4), 38 (2016). https://doi.org/10.3390/hydrology3040038
15. Huang, Q., Luzi, G., Monserrat, O., Crosetto, M.: Ground-based synthetic aperture radar interferometry for deformation monitoring: a case study at Geheyan Dam, China. J. Appl. Remote Sens. **11**(3), 1 (2017). https://doi.org/10.1117/1.JRS.11.036030
16. Hungr, O., Leroueil, S., Picarelli, L.: The Varnes classification of landslide types, an update. J. Appl. Remote Sens. **11**, 167–194 (2014). https://doi.org/10.1117/1.JRS.11.036030
17. Lague, D., Brodu, N., Leroux, J.: Accurate 3D comparison of complex topography with terrestrial laser scanner: application to the Rangitikei canyon (N-Z). ISPRS J. Photogramm. Remote. Sens. **82**, 10–26 (2013). https://doi.org/10.1016/j.isprsjprs.2013.04.009
18. Lee, K.L., Duncan, J.M.: Landslide of April 25, 1974 on the Mantaro River, Peru. National Academy of Sciences, Washington, DC (1975)
19. Lindenbergh, R., Pietrzyk, P.: Change detection and deformation analysis using static and mobile laser scanning. Appl. Geomatics **7**(2), 65–74 (2015). https://doi.org/10.1007/s12518-014-0151-y
20. Osmanoğlu, B., Sunar, F., Wdowinski, S., Cabral-Cano, E.: Time series analysis of InSAR data: methods and trends. ISPRS J. Photogramm. Remote Sens. **115**, 90–102 (2016). https://doi.org/10.1016/j.isprsjprs.2015.10.003
21. Awal, R., Nakagawa, H., Baba, Y., Sharma, R.H., Ito, N.: Study on landslide dam failure by sliding. Annuals of Disas. Prev. Res. Inst, Kyoto Univ., No. 50 B (2007)
22. Sattar, A., Konagai, K.: Recent Landslide Damming Events and Their Hazard Mitigation Strategies. In: Moustafa, A. (ed.) Advances in Geotechnical Earthquake Engineering – Soil Liquefaction and Seismic Safety of Dams and Monuments. InTech (2012). https://doi.org/10.5772/28044
23. Scaioni, M., Crippa, J., Longoni, L., Papini, M., Zanzi, L.: Image-based reconstruction and analysis of dynamic scenes in a landslide simulation facility. ISPRS Annals of the Photogrammetry, Remote Sensing and Spatial Information Sciences **IV-5/W1**, 63–70 (2017). https://doi.org/10.5194/isprs-annals-IV-5-W1-63-2017

24. Scaioni, M., et al.: Some applications of 2-D and 3-D photogrammetry during laboratory experiments for hydrogeological risk assessment. Geomat. Nat. Haz. Risk **6**(5–7), 473–496 (2015). https://doi.org/10.1080/19475705.2014.885090
25. Scaioni, M., Longoni, L., Zanzi, L., Ivanov, V., Papini, M.: Teaching geomatics for geohazard mitigation and management in the COVID-19 time. The International Archives of the Photogrammetry, Remote Sensing and Spatial Information Sciences **XLIV-3/W1-2020**, 131–138 (2020). https://doi.org/10.5194/isprs-archives-XLIV-3-W1-2020-131-2020
26. Scaioni, M., et al.: Analysis of spatial sensor network observations during landslide simulation experiments. Eur. J. Environ. Civ. Eng. **17**(9), 802–825 (2013). https://doi.org/10.1080/19648189.2013.822427
27. Scaioni, M., Marsella, M., Crosetto, M., Tornatore, V., Wang, J.: Geodetic and remote-sensing sensors for dam deformation monitoring. Sensors **18**(11), 3682 (2018). https://doi.org/10.3390/s18113682
28. Schuster, R.L.: Interaction of dams and landslides: case studies and mitigation. US Geol. Surv. (2006). https://doi.org/10.3133/PP1723
29. Schuster, R.L.: Risk-reduction measures for landslide dams. Ital. J. Eng. Geol. Environ. (2006). https://doi.org/10.4408/IJEGE.2006-01.S-01
30. Snow, D.: Landslide of Cerro Condor-Sencca, Department of Ayacucho, Peru. In: Kiersch, G.A. (ed.) Engineering Geology Case Histories Number 5, pp. 1–6. Geological Society of America, New York (1964). https://doi.org/10.1130/Eng-Case-5.1
31. Ivanov, I.V., et al.: Investigation on the role of water for the stability of shallow landslides—insights from experimental tests. Water **12**, 1203 (2020). https://doi.org/10.3390/w12041203
32. Vosselman, G., Maas, H.G.: Airborne and Terrestrial Laser Scanning. Taylor and Francis Group, Boca Raton, FL, USA (2010)
33. Fu-gang, X., Yang, Xing-guo, Zhou, Jia-wen, Hao, Ming-hui: Experimental research on the dam-break mechanisms of the Jiadanwan landslide dam triggered by the Wenchuan earthquake in China. Sci. World J. **2013**, 1–13 (2013). https://doi.org/10.1155/2013/272363
34. Doa, X.K., Kimb, M., Nguyenc, T., Jungd, K.: Analysis of landslide dam failure caused by overtopping. Procedia Eng. **154**, 990–994 (2016). https://doi.org/10.1016/j.proeng.2016.07.587